Formation of PdO on Au–Pd bimetallic catalysts and the effect on benzyl alcohol oxidation

Pingping Wu, Yunxiang Cao, Lianming Zhao, Yue Wang, Zhengke He, Wei Xing, Peng Bai, Svetlana Mintova, Zifeng Yan

Formation of PdO on Au-Pd bimetallic catalyst and the effect on benzyl alcohol oxidation

Pingping Wu,[†] Yunxiang Cao,[†] Lianming Zhao,[‡] Yue Wang,[†] Zhengke He,[†] Wei Xing,[‡] Peng Bai,[*,†] Svetlana Mintova,[†,μ] Zifeng Yan[†]

[†]State Key Laboratory of Heavy Oil Processing, CNPC Key Laboratory of Catalysis, College of Chemical Engineering, China University of Petroleum (East China), Qingdao 266580, China

[‡]School of Materials Science and Engineering, Institute of Advanced Materials, China University of Petroleum (East China), Qingdao, 266580, China.

[μ]Normandie University, ENSICAEN, UNICAEN, CNRS, Laboratoire Catalyse et Spectrochimie, 14000 Caen, France

* Corresponding authors. Tel: +86-532-86981812

E-mail address:*baipeng@upc.edu.cn (P. Bai)*

ABSTRACT

A series of catalysts containing of gold-palladium bimetallic nanoparticles (Au-Pd NPs in the range of 1-6 nm) anchored on foam-like mesoporous silica were used for the aerobic oxidation of benzyl alcohol. A remarkable synergistic effect was observed on these Au-Pd NPs catalysts prepared by one-pot method. Both the experimental and theoretical study revealed a close relationship between the surface PdO species on the catalysts and their catalytic performance, that is, a higher surface PdO content leads to a lower catalytic activity. The surface content of PdO species on the catalysts could be tuned by controlling the Au/Pd ratios, because the formation of Au-Pd alloy NPs and electron transfer between surface Au and Pd atoms prevented the oxidation of surface Pd and retarded the formation of PdO species. An optimal Au/Pd ratio of 1/4.5 on the foam-like mesoporous silica support was obtained, with nearly no surface PdO species formed and resulted the highest benzyl alcohol conversion of 96%. The bimetallic Au-Pd catalysts exhibited much higher catalytic activity for benzyl alcohol oxidation (TOF = 50000 - 60000 h^{-1}) than the monometallic Pd catalyst (TOF = 12500 h^{-1}) on which surface Pd is easily oxidized to PdO. These results provide direct evidence for the synergistic effect of the Au-Pd bimetallic catalyst in benzyl alcohol oxidation.

Keywords: *Au-Pd bimetallic catalyst, surface composition, synergistic effect, benzyl alcohol oxidation*

1. Introduction

The selective oxidation of alcohols on metal nanoparticles (NPs) to aldehydes or esters has attracted tremendous attention because the products play an important role in pharmaceuticals, agro-chemistry and cosmetics industries [1, 2]. In contrast to the conventional approach using stoichiometric amounts of chromate or permanganate as oxidants, the solvent-free liquid phase oxidation of alcohols with air, O_2 or H_2O_2 is recognized as a sustainable and environmentally friendly process, for the sole by-product is water. However, the major challenge for the application of solvent-free liquid oxidation in industry relies in the development of highly active and selective catalyst systems.

Supported noble metal NPs, such as Au [3-5], Pd [6, 7] and bimetallic catalysts (Au-Pd) [8-12] have been extensively studied for selective oxidation of alcohols [13]. Among them, gold (Au) and palladium (Pd) bimetallic catalyst was the most frequently reported for alcohol oxidation; a synergistic effect between these two metals was observed [8, 9, 14-16]. A particular “crown-jewel” structured Au-Pd bimetallic catalyst was synthesized by Toshima and co-workers and applied for glucose oxidation [17]. A much higher catalytic activity than those of monometallic Au and Pd NPs was observed in this “crown-jewel” structured Au-Pd catalyst. The synergistic effect was generally attributed to the collaborative effect (closely related to the local composition of Au/Pd) and electronic effect (electronic modification through hetero-nuclear metal-metal bond formation) [18-20]. Several works have been devoted to understand the synergistic effect in bimetallic catalysts. Chen and co-worker applied Au-Pd/$CeZrO_2$ catalyst for glycerol oxidation and they attributed the synergistic effect to the degree

of compositional homogenization [9]. A synergy effect was also observed on Au-Pd/$CeZrO_2$ catalyst for benzyl alcohol oxidation, which was ascribed to the electronic interaction between Au and Pd atoms [14]. The activity enhancement of Au atoms was also reported primarily by the variation in the occupation state of Pd d-orbitals [21]. Both the compositional homogenization and electronic interaction would lead to the alteration in occupation states of Pd d-orbitals, which seems to be the essence of the synergy effect, however the direct evidence is lacking. Furthermore, just on the opposite, an anti-

synergistic effect was observed in the bimetallic system by Hutchings et al. [14], which implies that the intrinsic mechanism of the synergy effect still remains elusive.

Among some studies on the Au-Pd bimetallic catalysts, the Au/Pd ratio was commonly observed to have significant effect on the catalyst performance. It was reported by Chen and co-workers that Au-Pd bimetallic catalyst with higher Au/Pd ratio exhibited better catalytic activity in the selective oxidation of glycerol [9]. A remarkably high catalytic activity using an Au-Pd core-shell catalyst with an Au/Pd ratio of 10:1 in benzyl alcohol oxidation was reported by Silva and coworkers [15]. Wang et al applied an atomic layer deposition method towards preparation of Au@Pd core–shell bimetallic catalyst. They found that the maximum benzyl alcohol conversion was obtained with a Pd shell thickness of 0.6–0.8 nm [16]. Recently, in Hutchings's work, the most active catalyst for benzyl alcohol oxidation had an Au/Pd ratio of 1 [14]. Among these works, a volcano-like relationship between catalyst activity and Pd content was recognized, and a maximum activity was observed at a certain Au/Pd ratio, which may vary depending on the different synthesis conditions. However, most of the works did not provide satisfactory explanations on this phenomenon. Wang et al attributed the effect of Pd shell thickness to both collaborative and electronic promotion, but without further

mechanistic investigation [16]. Based on the density functional theory (DFT) calculation, Silva et al. [15] explained that when Pd loading was high, the activity was enhanced because the increased number of Pd ensembles was favorable for the adsorption of benzyl alcohol. While further increase of Pd loading above the monolayer coverage, the adsorption of benzaldehyde was too strong, which impeded its desorption. The model was built based on the Au-Pd alloy without consideration of the possible existence of surface PdO species under oxidation conditions. Indeed, after oxidation at 250 ^{o}C, the formation of $Pd^{\delta+}$ species in both monometallic $Pd/CeZrO_2$ and bimetallic $AuPd/CeZrO_2$ catalysts was observed by Chen et al; the concentration of these species is higher in the monometallic $Pd/CeZrO_2$ [12]. However, no detailed investigation on different $Pd^{\delta+}$ contents in monometallic and bimetallic catalysts as well as their effect on the catalytic activity was carried out.

In this work, a series of Au-Pd bimetallic NPs catalysts supported on foam-like mesoporous silica were prepared with different Au/Pd ratios by a one-pot synthesis method, and applied for benzyl alcohol selective oxidation. In most cases, the formation of PdO species on Au-Pd NPs was identified even at room temperature in air atmosphere. The content of PdO was tuned by varying the Au/Pd ratios. The relationship between the catalyst activity and the PdO content was experimentally and theoretically studied.

2. Experimental

2.1. Chemicals

$HAuCl_4 \cdot xH_2O$ (Sinopharm Chemical), $PdCl_2$ (Sinopharm Chemical), triblock co-polymer $PEO_{20}PPO_{70}PEO_{20}$ (P123, Aldrich), tetraethyl orthosilicate (TEOS, 98%, Sinopharm Chemical), mercaptopropyltrimethoxysilane (MPTMS, 97%, Aldrich), 1,3,5-trimethylbenzene (99%, Sinopharm

Chemical), hydrochloric acid (37%, Sinopharm Chemical), benzyl alcohol (99.99%, Sinopharm Chemical), benzaldehyde (99.99%, Sinopharm Chemical), benzoic acid (99.99%, Sinopharm Chemical) and absolute ethanol (99.98%, Sinopharm Chemical) were used as received without further purification.

2.2. Preparation of catalysts

The mesoporous silica support was synthesized by methods reported previously [22, 23]. The noble metal precursors were introduced during the synthesis of mesoporous silica support, which has been reported in our previous work [24, 25]. Typically, 4 g of P123 was dissolved in a mixture of 65 mL deionized water and 5 mL 37% HCl at room temperature. Then, 3g of 1,3,5-trimethylbenzene was added into the clear solution as a pore swelling agent and stirred at 40 ^{o}C for 2 h， followed by addition of 8.32 g of TEOS and 0.78g of MPTMS drop wise into the mixture. Finally, the $HAuCl_4$ and $PdCl_2$ solutions (the metal loading of 1 wt. %) were introduced in the synthesis mixture. After stirring at 40 ^{o}C for 24 h, the mixtures were transferred to a Teflon-lined stainless-steel autoclave to undergo a hydrothermal treatment at 100 ^{o}C for 24 h. After the crystallization was accomplished, the solids were purified with deionized water, dried under vacuum at 80 ^{o}C overnight and finally calcined in air at 500 ^{o}C for 6 h. The calcined samples were further treated under H_2 at 400 ^{o}C for 2h. The catalysts with a total metal loading of 1*wt.*% were abbreviated as Au_xPd_y/MCF-H_2 (*x*, *y* represent the molar percentages of Au and Pd, respectively): samples Au_{100}/MCF, Au_8Pd_{92}/MCF-H_2, $Au_{18}Pd_{82}$/MCF-H_2, $Au_{26}Pd_{74}$/MCF-H_2, $Au_{61}Pd_{39}$/MCF-H_2 and Pd_{100}/MCF-H_2. The catalysts with a total metal loading of 2*wt.*% were abbreviated as 2*wt.*%Au/MCF-H_2, 1*wt.*%Au-1*wt.*%Pd/MCF-H_2 and 2*wt.*%Pd/MCF-H_2. Additionally, a sample under static air calcination at 500 ^{o}C for 1 h was prepared to evaluate the effect

of treatment under different atmosphere (sample $Au_{26}Pd_{74}/MCF\text{-}O_2$) and compared with the original sample $Au_{26}Pd_{74}/MCF\text{-}H_2$.

2.3. Characterization

N_2 adsorption/desorption was carried out to analyze the textural property of catalysts degassed at 300 ºC for 4 h under vacuum using an automatic volumetric sorption analyzer (Micromeritics, TriStar 3000). The specific surface area was calculated using the Brunauer-Emmett-Teller (BET) equation at the relative pressure of 0.05-0.25. The total pore volume of catalysts was obtained at the relative pressure P/P_0 of 0.989. The Barrett-Joyner-Halenda (BJH) equation was used to obtain the pore size distribution using the desorption branch of the isotherm. X-ray powder diffraction (XRD) patterns of catalysts were recorded on a X'Pert PRO MPD system with a Cu *Kα* radiation (λ = 0.154 nm) at 35 kV and 40 mA. Wide-angle X-ray scattering was recorded from 20° to 85° 2Theta with a scanning rate of 5° per minute. Noble metal loadings in the catalysts were determined by inductively coupled plasma optical emission spectroscopy (ICP-OES) using a VISTA-MPX Varian system. The ultraviolet-visible (UV-vis) spectra analysis of catalysts was performed on a HitachiU-4100 UV-vis-NIR spectrophotometer using $BaSO_4$ as an internal reference. The diffusion reflectance spectra from 350 to 800 nm were recorded.

The microstructure of the catalysts was characterized by high-resolution Transmission Electron Microscope (HRTEM) using a JEM 2010 JEOL operated at 200 kV. Based on the TEM images of the Au-Pd bimetallic catalysts, diameters of more than 150 metal particles randomly selected were measured, and the average particle diameter was calculated based on following equation: $d=\Sigma nidi/\Sigma ni$, where $ni \geq 150$. The metal dispersion was calculated using GAUSS software from Nanomaterials and

Catalysis Group of University of Cadiz (Spain) assuming a spherical particle shape [26]. Scanning transmission electron microscopy (STEM) high angle annular dark field (HAADF) images and X-ray energy dispersive spectra (XEDS) of the metallic particles were applied to analyze the distribution and elements dispersion of Au and Pd NPs. Additionally, tomography data were obtained using a FEI Tecnai F30 electron microscope operating at 300 kV. Colloidal gold particles (10 nm) were used as a marker in the TEM study. The tomographic series were carried out by tilting the specimen around a single axis from 50 ° to –50 ° at an increment of 1º under the electron beam. Data processing was carried out by the IMOD software.

The surface property and relative proportions of elements in the catalysts were investigated by X-ray photoelectron spectroscopy (XPS). The XPS analyses were performed on a Thermo-VG Scientific K-Alpha spectrometer equipped with an Al anode (Al Ka = 1486.6 eV). C 1s electron bond energy corresponding to graphitic carbon at 284.5 eV was applied as a calibration binding energy (BE) reference. The reducibility of catalysts was measured by hydrogen temperature programmed reduction using a Chem-BET 3000 TPD/TPR analyzer (Autochem Ⅱ, USA). Before analysis, the samples were degassed at room temperature for 4 h and the signals were recorded from 40 ºC to 600 ºC with a heating rate of 20 ºC /min.

2.4. Catalytic test

Solvent-free aerobic oxidation of benzyl alcohol with O_2 as oxidant was performed in a 100 mL autoclave liner with a polytetrafluoroethylene (Model: SLM100, Beijing Easychem Science and Technology Development Company, China). Typically, 10.8 g benzyl alcohol and 50 mg solid catalyst were introduced in the reactor. After purging with O_2 three times, the reactor was heated to 110 ºC and

the O_2 pressure was adjusted to 0.8 MPa under stirring. The O_2 pressure was kept at 0.8 MPa during the entire reaction. After 1 h of reaction, the reactor was cooled down in an ice bath to 30 ºC and the pressure was released. Then the reactor was opened slowly and the reaction products were separated by centrifuge. The solid catalyst was washed with ethanol and dried at 80 ℃ prior the next catalytic experiment. The n-pentanol was added to the reaction products as an internal standard. Finally, the reaction products were analysed using a gas chromatogram (Agilent 6870) equipped with an FID detector and a DB-1 column (30*0.32*0.25). The turnover frequency (TOF) was calculated based on moles of benzyl alcohol converted per mole of surface metals (Au + Pd) per hour, e.g., $M_{BA\ converted}\ h^{-1} M_{\ surface\ metal}^{\ -1}$, while the amount of surface metals (Au + Pd) was calculated based on the total moles of metals multiplied by the metal dispersion.

2.5. Theoretical study

All first-principle calculations were carried out using the periodic density functional theory (DFT) method with the Perdew-Burke-Ernzerh (PBE) form of the general gradient approximation (GGA) functional in the DMol^3 package. The ion cores of Pd and Au atoms were treated by the density functional semicore pseudopotential (DSPP), while the valence electrons were described by the double-numerical basis with polarization functions (DNP). The Fermi smearing and real space cutoff were set to 0.005 hartree and 4.7 Å, respectively. The convergence tolerances were set to 5×10^{-3} Å for displacement, 2×10^{-3} hartree/Å for gradient, and 1×10^{-5} hartree for total energy. In addition, the spin-polarization was employed in all calculations.

The calculated adsorption energy is presented as follows, $E_{ads} = E_{adsorbate/substrate} - (E_{adsorbate} + E_{substrate})$,

where E_{ads} is the adsorption energy of the adsorbate on metal surfaces, $E_{adsorbate/substrate}$ is the total energy of the slab with an adsorbed molecule, and $E_{adsorbate}$ and $E_{substrate}$ are the energies of the free adsorbate and the clean slab, respectively. For example, the oxygen adsorption energy was calculated using the following equation: $E_{ads} = E_{sub+O^*} - E_{sub} - 1/2E_{O_2}$, where E_{sub+O^*}, E_{sub}, $1/2E_{O_2}$ are the total energy after O adsorption, the energy of the catalyst substrate, and one-half of the energy of a free oxygen molecule, respectively.

3. Results

3.1. Textural properties of Au-Pd bimetallic catalysts

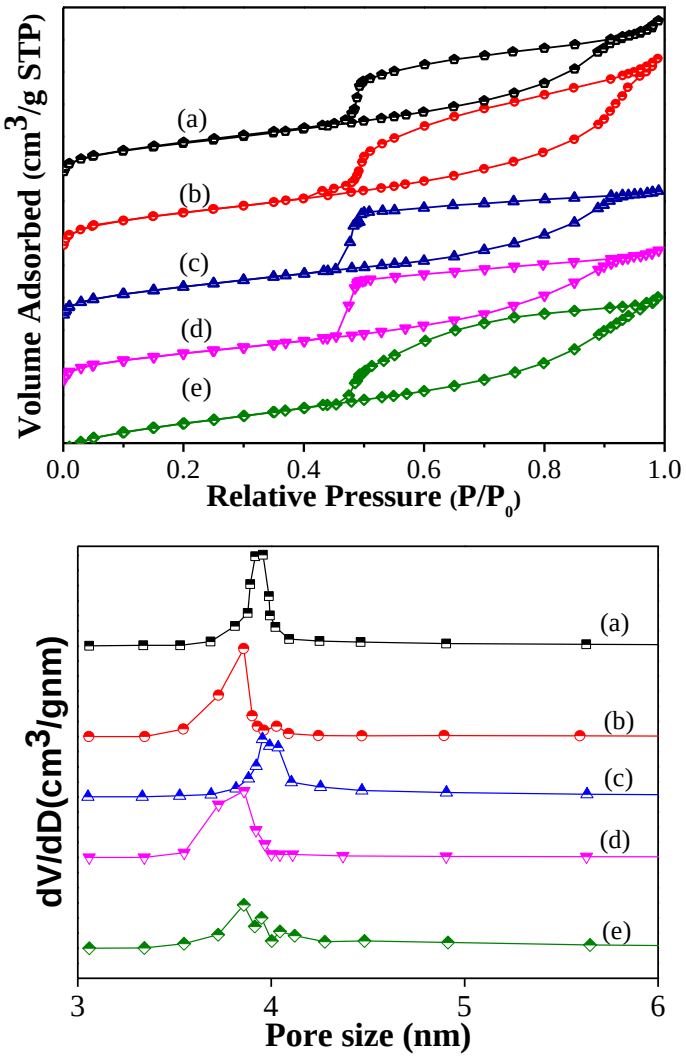

Fig. 1. N_2 adsorption-desorption isotherms (left) and pore size distribution curves (right) of Au-Pd

bimetallic catalysts: (a) Au_8Pd_{92}/MCF-H_2, (b) $Au_{18}Pd_{82}$/MCF-H_2, (c) $Au_{26}Pd_{74}$/MCF-H_2, (d) $Au_{61}Pd_{39}$/MCF-H_2 and (e)Au_{100}/MCF-H_2.

The N_2 adsorption-desorption isotherms and pore size distribution curves of Au-Pd bimetallic catalysts are shown in Fig. 1, Fig. S1 (SI) and Table 1. According to IUPAC classification, all catalysts exhibit a type-IV isotherm related to the H-2 hysteresis loop suggesting that all catalysts possess ink-bottle mesopores. The shape of the hysteresis loop of the Au-Pd bimetallic catalysts deviates from the H-1 loop which is typically observed for pure MCF-17 and this is probably due to the addition of MPTMS during the synthesis. The MPTMS may disturb the formation and self-assembly process and lead to distortion of the mesopore structure of the catalysts. Additionally the introducing of Au-Pd NPs may change the pore shape of the MCF-17 [27]. The hysteresis loop for all Au-Pd catalysts (Fig. 1) is observed at a relative pressures, P/P_0 of 0.4–0.5, indicating the presence of small mesopores. The pore size distribution of all catalysts are in the similar range of 3～5 nm. A high specific surface area above > 650 m^2/g was measured for all samples, while sample $Au_{26}Pd_{74}$Pd/MCF-O_2 shows the highest specific surface area (737 m^2/g). No relationship between the Au/Pd ratios or treatment conditions and porosity of samples was observed.

3.2 Morphology and crystalline structure of Au-Pd bimetallic catalysts

TEM images and particle size distribution histograms of Au-Pd/MCF catalysts are shown in Fig. 2 and Fig. S1. The metal loading, particle diameter and metal dispersion of catalysts are summarized in Table 1. Well dispersed noble metal NPs (1-6 nm) were observed in both monometallic and bimetallic catalysts. Sample Au_{100}/MCF exhibited the highest metal dispersion (46 %) among all catalysts as shown in Fig. 2f and Table 1. With an increase of the Pd ratio, the average particle diameter increased and metal dispersion decreased, indicating that the addition of Au to Pd improved the metal

dispersion on the mesoporous silica support.

The crystalline structure of NPs treated under different atmospheres were studied by HRTEM. Fig. 2g and 2h present the $Au_{26}Pd_{74}$/MCF-H_2 and $Au_{26}Pd_{74}$/MCF-O_2 catalysts, respectively. Metal NPs with a lattice spacing of 0.227-0.231 nm were observed, which is between the values of Au (111) (0.235 nm in JCPDS card: 04-0784) and Pd (111) (0.225 nm in JCPDS card: 65-2867) [28, 29]. This suggests the alloying of Au and Pd NPs in sample $Au_{26}Pd_{74}$/MCF-H_2 obtained under H_2 reduction. While in sample $Au_{26}Pd_{74}$/MCF-O_2, a high portion of metal NPs with a lattice spacing of 0.213-0.214 nm, indicating the formation of PdO (0.212 nm) with (200) plane of (JCPDS card: 02-1432) were measured.

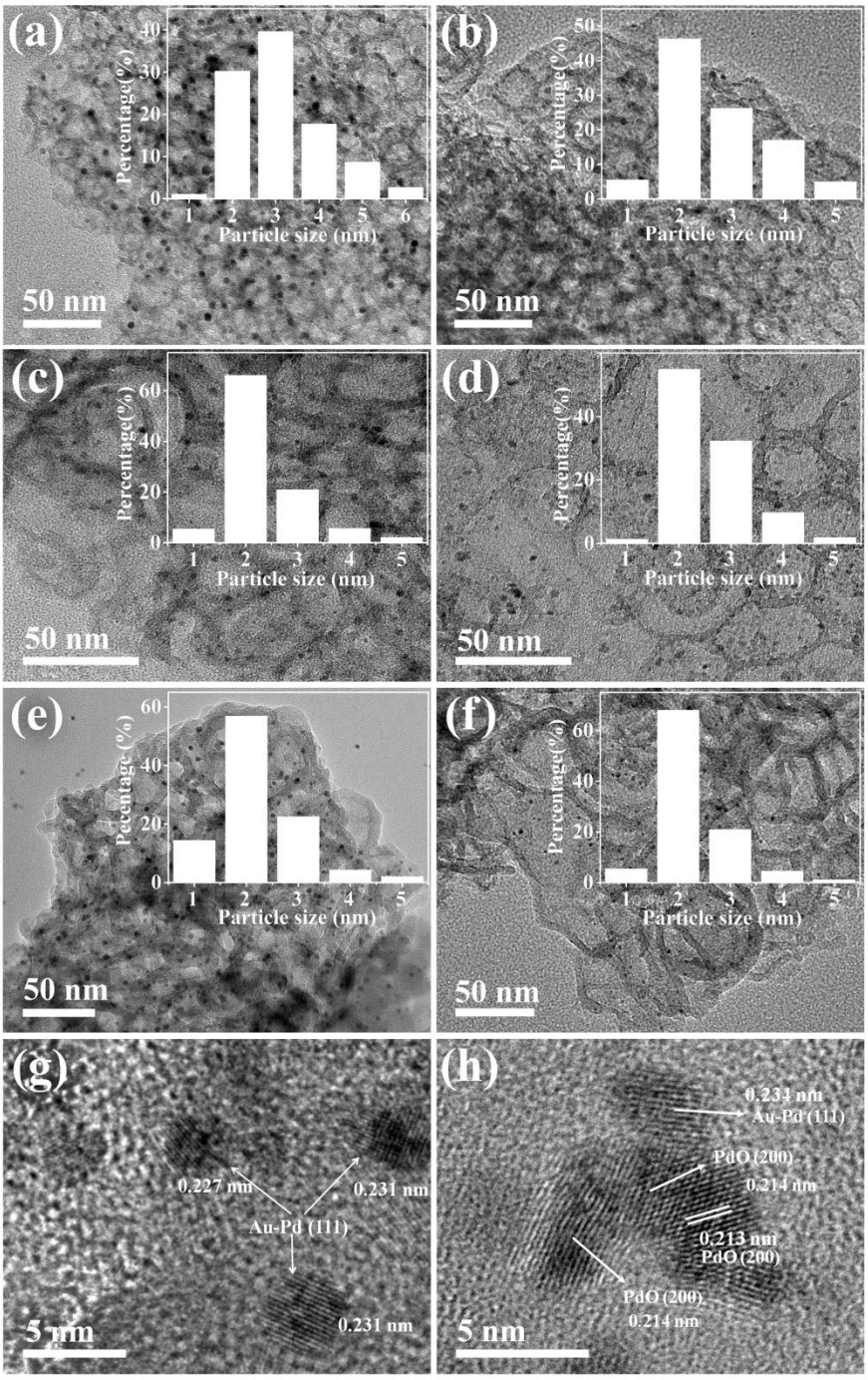

Fig. 2. TEM images and particles size distribution histograms of catalysts: (a) Au_8Pd_{92}/MCF-H_2 (b) $Au_{18}Pd_{82}$/MCF-H_2, (c) $Au_{26}Pd_{74}$/MCF-H_2, (d) $Au_{26}Pd_{74}$/MCF-O_2, (e) $Au_{61}Pd_{39}$/MCF-H_2, (f) Au_{100}/MCF-H_2 (g)$Au_{26}Pd_{74}$/MCF-H_2 and (h) $Au_{26}Pd_{74}$/MCF-O_2.

As shown in the XRD patterns in Fig. S2, very weak diffraction peaks corresponding to bimetallic Au-Pd NPs appeared. The XRD patterns of samples loaded with 2*wt.*% NPs (2*wt.*%Au/MCF-H_2,

1*wt*.%Au-1*wt*.%Pd/MCF-H_2 and 2*wt*.%Pd/MCF-H_2) are shown in Fig. S3. Four diffraction peaks at 38.2, 44.4, 64.7 and 77.7^o 2Theta corresponding to (111), (200), (220), (311) planes of cubic Au (PDF#65-8601), respectively in sample 2%Au/MCF-H_2 were measured. While no cubic Pd phase was observed in sample 2*wt*.%Pd/MCF-H_2, instead, PdO phase (PDF#06-0515) was found, which is probably due to the oxidation of Pd in air. Four peaks at 40.1, 46.6, 68.1, and 82.1^o 2Theta corresponding to the (111), (200), (220), (311) planes of cubic Pd (PDF#65-2867), respectively were expected but not observed. While slight shift of the Bragg peaks to higher 2Theta region for the 1*wt*.%Au-1*wt*.%Pd/MCF-H_2 in comparison to the 2*wt*.%Au/MCF-H_2, was measured. These results clearly show the formation of Au-Pd alloy NPs in sample 1*wt*.%Au-1*wt*.%Pd/MCF-H_2 [30]. No diffraction peaks assigned to PdO phase were detected in this sample (1*wt*.%Au-1*wt*.%Pd/MCF-H_2), indicating that the formation of Au-Pd alloy NPs may prevent the oxidation of Pd in air.

3.3. Electron tomography (ET) analysis of Au-Pd bimetallic catalysts

The presence of well-dispersed noble metal NPs in foam-like silica support was confirmed by HRTEM. But the exact spatial location of the noble metal NPs either inside the pores or on the external surface of the silica surface is still unknown. It is known that the location and stability of noble metal NPs are directly related with their catalytic activity. The HRTEM only provides a two-dimensional image, resulting often in misleading spatial information. Therefore, electron tomography (ET), a 3D analysis, was employed to reveal the spatial location of noble metal NPs in the porous silica support; the results are shown in Fig. 3. Fig. 3a displays the TEM image of sample $Au_{26}Pd_{74}$/MCF-H_2. The large black points in Fig. 3a are colloidal gold particles (10 nm) which were used as marker for the TEM study. The well-defined foam-like structure can be clearly seen by the full range tilting video (SI, Video 1: scale bar 100 nm). Fig. 3b and 3c show the ET tomograms sliced at different thicknesses (full

range tomogram video slicing from the bottom to the top of the catalyst is provided in SI; Video 2: scale bar 50 nm). No aggregation of noble metal NPs was observed, only separated and well-dispersed dots with an average size of around 3 nm are seen in the porous silica support. This indicates that no aggregation of the NPs treated at 500 ^{o}C occurred. The noble metal NPs are observed not only on the silica surface (indicated by red arrows in Fig. 3b, 3c) but also embedded within the silica wall (indicated by white cycles in Fig. 3b, 3c). The homogeneous distribution of NPs in the silica support is due to the in-situ incorporation of gold during the preparation of foam-like silica support. The ET tomograms sliced at different thicknesses of the sample indicate that the metal NPs are attached on the silica wall surface, which will be conducive to the catalytic stability. The high porosity of the foam-like silica support was retained which is beneficial for the diffusion of reactants into the pores. The restructured 3D structures of three neighboring mesopores containing Au-Pd NPs (colored cycles highlighted in Fig. 3c) is also shown in Fig. 3d. This result provides a direct visualization of the distribution of metal particles within the silica foam. The Au-Pd NPs without aggregation (pink color) are anchored on the pore walls (yellow blue and green colors).

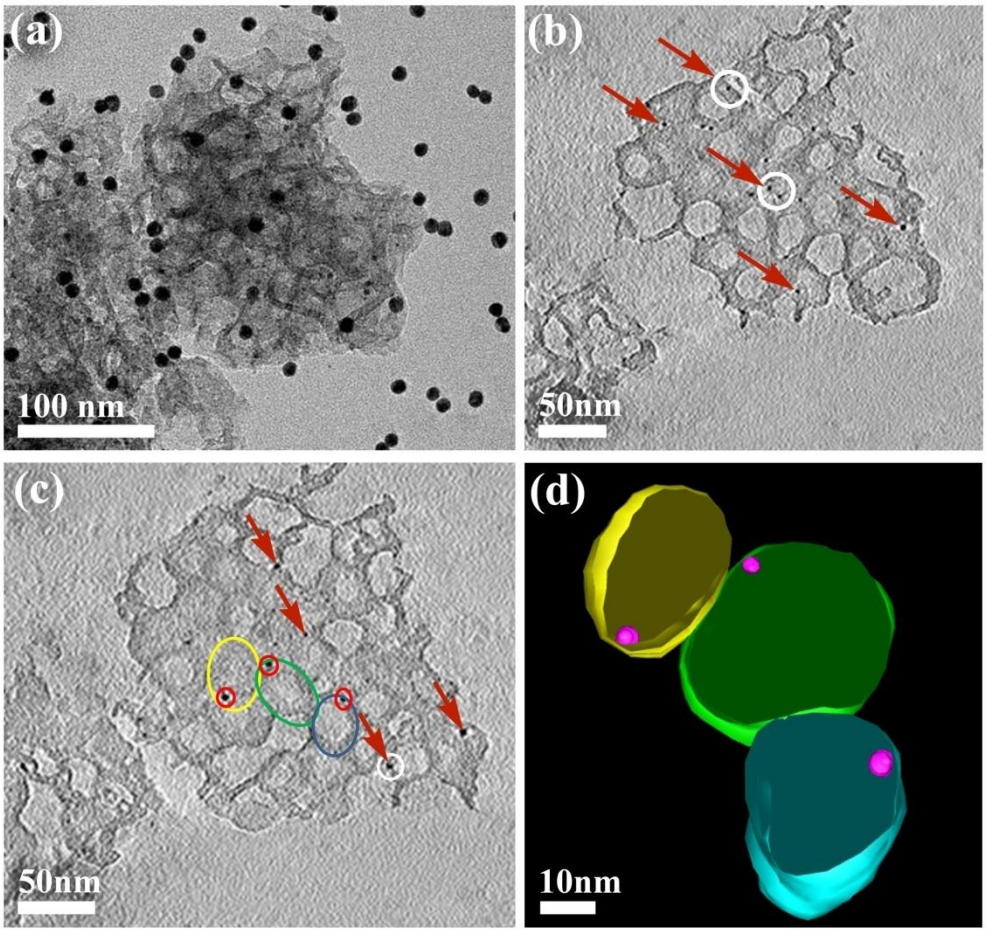

Fig. 3. (a) TEM images of sample $Au_{26}Pd_{74}$/MCF-H_2, (b-c) electron tomograms sliced at different thicknesses, (d) reconstructed 3D structure of three neighboring cages containing Au-Pd nanoparticles.

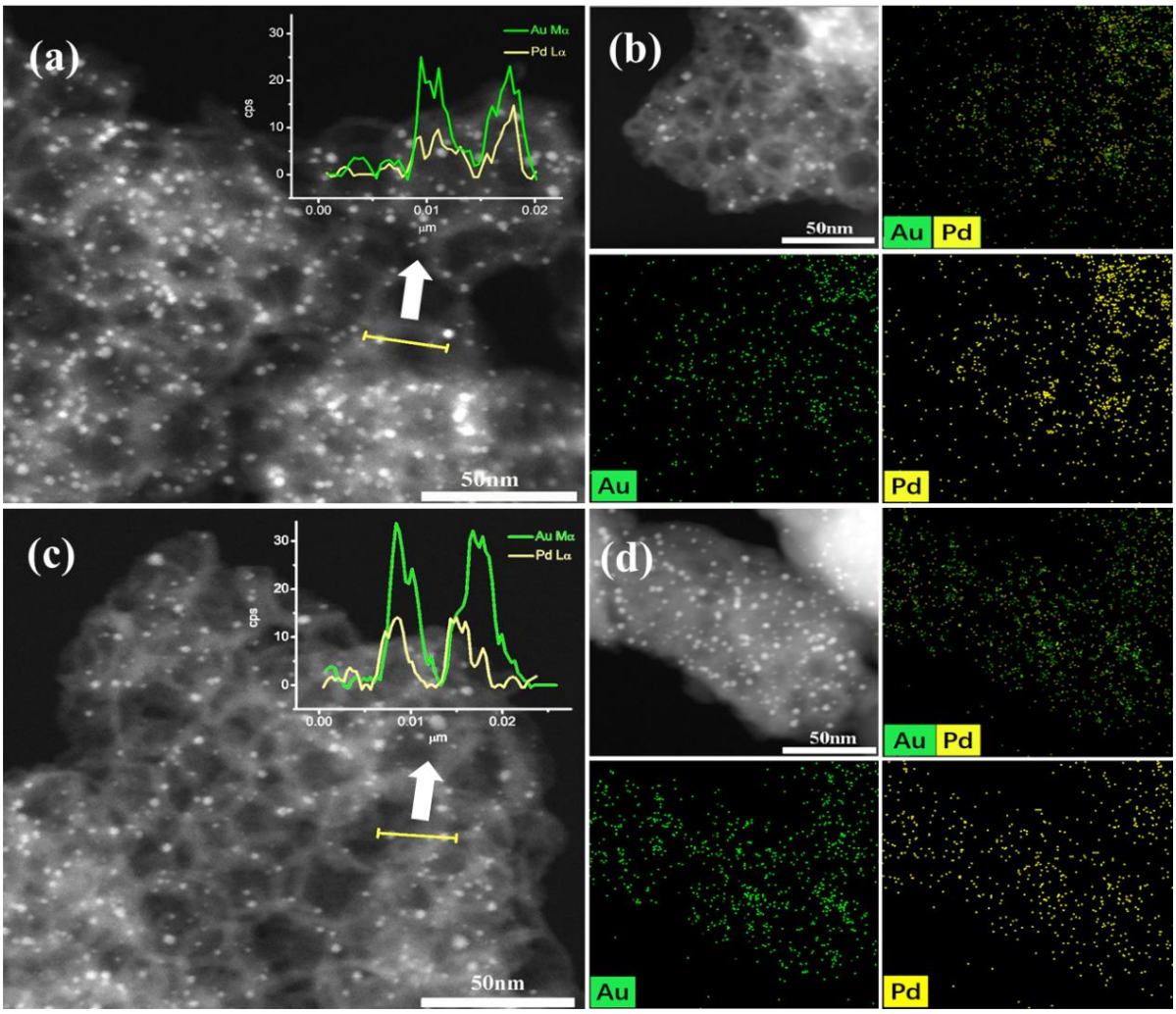

Fig. 4. (a) STEM-HAADF image of $Au_{26}Pd_{74}$/MCF-H_2 (insert is the energy dispersive line scan across NPs. using the Au-M and Pd-L X-rays), (b) representative STEM images and the corresponding color-coded EDS spectral maps of Au (green), Pd (yellow) and Au-Pd, (c) STEM-HAADF image of $Au_{26}Pd_{74}$/MCF-O_2 (insert is the energy dispersive line scan across NPs using the Au-M and Pd-L X-rays), and (d) representative STEM images and corresponding color-coded EDS spectral maps of Au (green), Pd (yellow) and Au-Pd.

3.4. STEM-HAADF characterization of Au-Pd bimetallic catalysts

The elemental distribution within the catalysts has a profound effect on their catalytic performance as was previously revealed by STEM [12, 31]. Fig. 4 shows the representative STEM-HAADF images and the corresponding colour-coded EDS spectral maps of $Au_{26}Pd_{74}$/MCF-H_2 and

$Au_{26}Pd_{74}$/MCF-O_2 catalysts. Well dispersed metal NPs on foam-like porous silica were seen on both catalysts subjected to H_2 or static air treatments (Fig. 4a and 4c). EDS mapping shows that both Au (green) and Pd (yellow) elements are well distributed and aligned thus indicating the formation of Au-Pd alloy NPs. The ratios of the peaks corresponding to the amount of Au and Pd in the bimetallic catalyst reveal that each NP has a similar Au/Pd ratio (see insert in Fig. 4 a,c). The STEM-EDS mapping results of analysed area are presented in Fig. S4 and Fig. S5, the weight percentages of Au and Pd in the analysed area of catalyst $Au_{26}Pd_{74}$/MCF-H_2 are 0.58 wt. % and 0. 62 wt. %, while on catalyst $Au_{26}Pd_{74}$/MCF-O_2 are 0.49 wt. % and 0.63 wt. %, respectively, quite consistent with ICP results (0.39% and 0.58% for Au and Pd, respectively, as shown in Table 1).

Table 1

Physical properties of catalysts.

Catalysts	ICP Au[a] (wt. %)	ICP Pd[a] (wt. %)	S_{BET} (m^2/g)	Pore volume (cm^3/g)	Pore size (nm)	Particle size [b] (nm)	Average particle diameter [c] (nm)	Metal dispersion [d] (%)
$Pd_{100}/MCF\text{-}H_2$ [e]	0.0	0.89	694	0.96	4.0	1-6	3.2±0.1	35
$Au_8Pd_{92}/MCF\text{-}H_2$	0.13	0.86	652	0.84	4.0	1-6	3.1±0.2	37
$Au_{18}Pd_{82}/MCF\text{-}H_2$	0.32	0.70	701	0.92	4.0	1-5	2.9±0.1	39
$Au_{26}Pd_{74}/MCF\text{-}H_2$	0.39	0.59	715	1.00	4.0	1-5	2.7±0.1	42
$Au_{61}Pd_{39}/MCF\text{-}H_2$	0.60	0.21	734	0.91	3.9	1-5	2.6±0.1	43
$Au_{100}/MCF\text{-}H_2$	0.94	-	730	0.91	4.0	1-5	2.5±0.2	46
$Au_{26}Pd_{74}/MCF\text{-}O_2$[e]	0.39	0.59	737	0.97	3.9	1-5	2.7±0.2	42

[a]: The metal content was measured by ICP-OES. [b,c]: The particle size distribution and average particle diameter were measured by TEM, counting 150～200 particles. [d]: The metal dispersion was calculated by GAUSS. [e]: The N_2 adsorption/desorption isotherm and TEM images of catalysts $Pd_{100}/MCF\text{-}H_2$ and $Au_{26}Pd_{74}/MCF\text{-}O_2$ are shown in Fig. S1.

3.5. UV-vis spectroscopy study of Au-Pd bimetallic catalysts

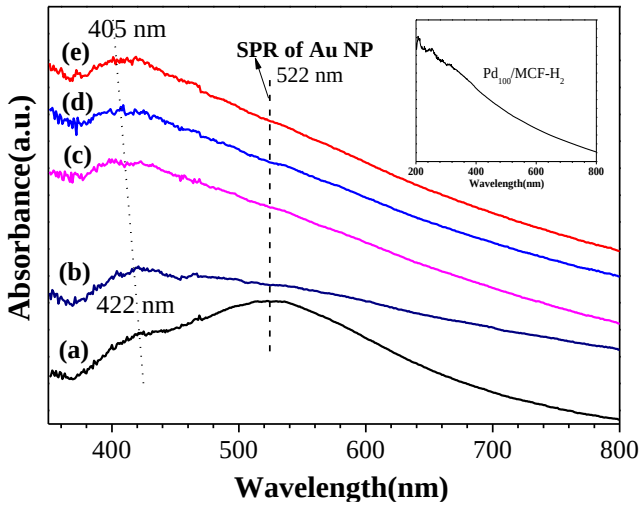

Fig. 5. UV-vis spectra of catalysts with different Au/Pd ratios: (a) Au_{100}/MCF-H_2, (b) $Au_{61}Pd_{39}$/MCF-H_2, (c) $Au_{26}Pd_{74}$/MCF-H_2, (d) $Au_{18}Pd_{82}$/MCF-H_2, (e) Au_8Pd_{92}/MCF-H_2, and Pd_{100}/MCF-H_2 (inset).

UV-vis spectra of Au-Pd/MCF catalysts are shown in Fig. 5. The Au_{100}/MCF-H_2 sample showed two broad peaks at 420 nm and 520 nm. The latter peak is associated with the surface plasmon resonance (SPR) of Au^0 NPs [32], whereas the former peak is assigned to the partially charged Au_n clusters [33]. The Pd_{100}/MCF-H_2 catalyst does not show any SPR band between 200 nm and 800 nm (see inset of Fig. 5). Introducing 0.2 *wt*.% Pd ($Au_{61}Pd_{39}$/MCF-H_2) led to significant broadening or even disappearance of the Au SPR band (520 nm). However, the peak at 420 nm was enhanced and shifted to lower wavelength. As the Pd/Au ratio increased, a decrease of the Au^0 NPs and an increase of partially charged Au_n clusters in the bimetallic catalysts was measured. These results indicate the surface electron variation of Au NPs after introducing Pd as a promoter, which is probably due to the formation of Au-Pd alloy NPs and the presence of surface electron transfer between Au and Pd. This statement would be further confirmed by XPS data.

3.6. XPS analysis of Au-Pd bimetallic catalysts

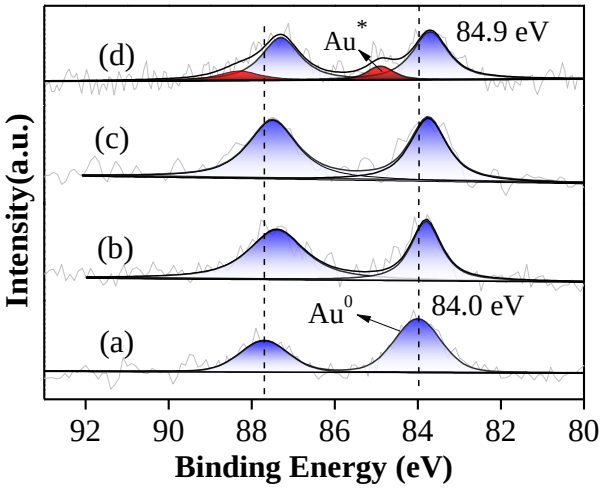

Fig. 6. XPS spectra of Au 4f of different catalysts: (a) Au_{100}/MCF-H_2, (b) $Au_{61}Pd_{39}$/MCF-H_2, (c) $Au_{26}Pd_{74}$/MCF-H_2 and (d) $Au_{18}Pd_{82}$/MCF-H_2.

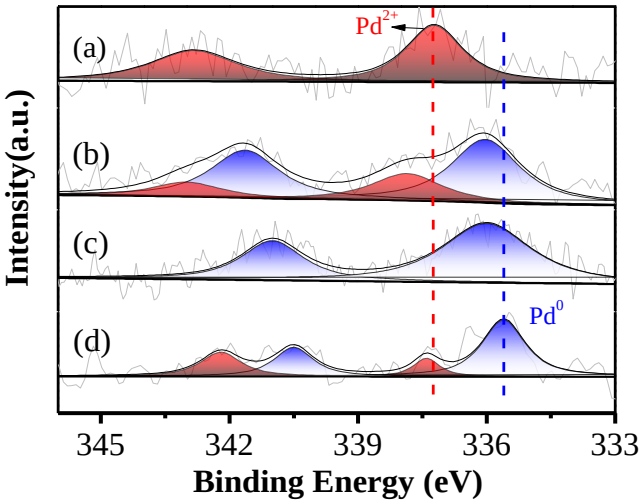

Fig. 7. XPS spectra of Pd 3d of different catalysts: (a) Pd_{100}/MCF-H_2., (b) Au_8Pd_{92}/MCF-H_2, (c) $Au_{18}Pd_{82}$/MCF-H_2 and (d) $Au_{26}Pd_{74}$/MCF-H_2.

The electronic properties of the Au-Pd bimetallic NPs were characterized by XPS. XPS spectra of Au 4f and Pd 3d are shown in Fig. 6 and Fig. 7, respectively. As shown in Fig. 6, typical Au^0 species [34-36] with binding energy (BE) of 84.0 eV (Au4$f_{7/2}$) and 87.8 eV (Au4$f_{5/2}$) were observed on catalyst Au_{100}/MCF-H_2 (Fig. 6a). Comparing to the pure Au sample, the Au 4f peaks for Au-Pd bimetallic catalysts shift downward in BE by 0.2～0.3 eV (4$f_{7/2}$ 83.7 eV and 4$f_{5/2}$ 87.5 eV) with an increase of the Pd introduced. This is attributed to

charge transfer between Pd and Au, indicating that the electronic structure of the surface Au atoms was modified upon the addition of Pd, and negatively charged Au species were obtained. It is interesting to note that two doublets at higher BEs of 84.9 eV and 88.3 eV were observed for the $Au_{18}Pd_{82}$/MCF-H_2 catalyst. It was reported that this positive shift of Au BE was due to the presence of sub-nano size Au^{0*}clusters or positively charged $Au^{\delta+}$ species, which is still under debate [37]. The Au^{0*} or $Au^{\delta+}$ species found on the Au catalyst surface was reported to enhance the catalytic activity of supported gold NPs catalyst for low temperature CO oxidation [38]. In our previous work, it was also found that the surface $Au^{\delta+}$ sites acted as active species for O_2 activation during non-solvent cyclohexane oxidation [39]. Thus, the presence of these active sites on the $Au_{18}Pd_{82}$/MCF-H_2 catalyst may lead to high catalytic activity for benzyl alcohol oxidation. The results from the catalytic test are presented below.

The Pd 3d spectra of different catalysts were shown in Fig. 7. Fig. 7a shows the Pd 3d peaks for sample Pd_{100}/MCF-H_2 at 337.2 eV and 342.8 eV, which are assigned to the surface Pd^{2+} species [40]. The presence of 100 % Pd^{2+} in sample Pd_{100}/MCF is due to the easy oxidation of Pd to PdO in air or water at room temperature during storage or characterization step [13]. The presence of PdO on the pure Pd catalyst was also confirmed by the XRD characterization (Fig. S3). The spectra of the Au-Pd bimetallic catalysts were fitted by two doublets: the higher Pd $3d_{5/2}$ energy value of Pd^{2+} (～337.2 eV) [41, 42] and the lower energy value of metallic Pd^0 (～335.5 eV) [16], showing that the percentage of oxidized Pd^{2+} decreased dramatically. Focusing on the Pd $3d_{5/2}$ with a BE of 335.5 eV on catalyst $Au_{26}Pd_{74}$/MCF-H_2 (Fig. 7d), it is clearly noted that this peak is gradually shifted to higher BE with increasing the Pd/Au ratio. This positive shift of Pd^0 BE on Au-Pd bimetallic catalysts indicates that the redistribution of electrons is occurred, leading to the formation of positively charged surface $Pd^{\delta+}$ atoms. Comparing the XPS results, the negative shift of Au 4f peaks and positive shift of Pd 3d peaks clearly indicate the transfer of electrons from Pd to Au on the bimetallic catalysts.

In addition, the fraction of Pd^{2+} to metallic Pd^0 species in the bimetallic catalysts was calculated by the peak

fitting and presented in Table 2. By comparing the relative intensity of the palladium oxide (PdO) and palladium metal (Pd) components in bimetallic catalysts, it was found that the PdO/Pd ratio decreased with the increase of the Au/Pd ratio. This indicates that alloying with Au prevent the surface Pd^0 to be oxidized to Pd^{2+} species, which is consistent with Yang's research results [9, 43]. The XPS results provide information on the surface metal ratios of Au/Pd and PdO/Pd , while the ICP results indicate the bulk Au/Pd ratios (Table 2). A relationship between the surface ratios of Au/Pd and PdO/Pd was observed. Catalyst $Au_{18}Pd_{82}$/MCF exhibited a steady surface and bulk Au/Pd atomic ratio of 0.22, and no PdO species were measured (three parallel XPS analyses were performed). However, the $Au_{26}Pd_{74}$/MCF-H_2 catalyst has much lower surface Au/Pd (0.27) than bulk (0.36) ratios with the presence of PdO species. Furthermore, the $Au_{26}Pd_{74}$/MCF-H_2 catalyst was treated in static air at 500 ^oC for 1 h (catalyst denoted as $Au_{26}Pd_{74}$/MCF-O_2) to justify the relation between surface PdO species and surface Au/Pd ratio. XPS results shown in Fig. 8 indicate the presence of certain amount of Pd^{2+} phase (12 %) in the $Au_{26}Pd_{74}$/MCF-H_2 catalyst, which is probably due to the easy oxidation of surface Pd atoms during the sample treatment. While in the $Au_{26}Pd_{74}$/MCF-O_2, the percentage of Pd^{2+} was notably enhanced to 38 %. The PdO/Pd ratio (0.61) for the $Au_{26}Pd_{74}$/MCF-O_2 was much higher than in the $Au_{26}Pd_{74}$/MCF-H_2 (0.19). Simultaneously, the surface Au/Pd ratio decreased from 0.27 to 0.14, implying the enrichment of PdO species on the surface of the bimetallic NPs after oxidation in static air. The presence of PdO species on the bimetallic catalysts leads to a lower amount of surface Au; this is due to the enrichment of PdO species on the surface of Au-Pd alloy NPs and covering of the Au sites. Anyhow, compared with the pure Pd_{100}/MCF-H_2 sample (100 % PdO), the percentage of PdO in the $Au_{26}Pd_{74}$/MCF-O_2 is still lower even after oxidation at 500 ^oC for 1h (38 % PdO), indicating that the formation Au-Pd alloy prevented the easy oxidation of Pd^0 atoms.

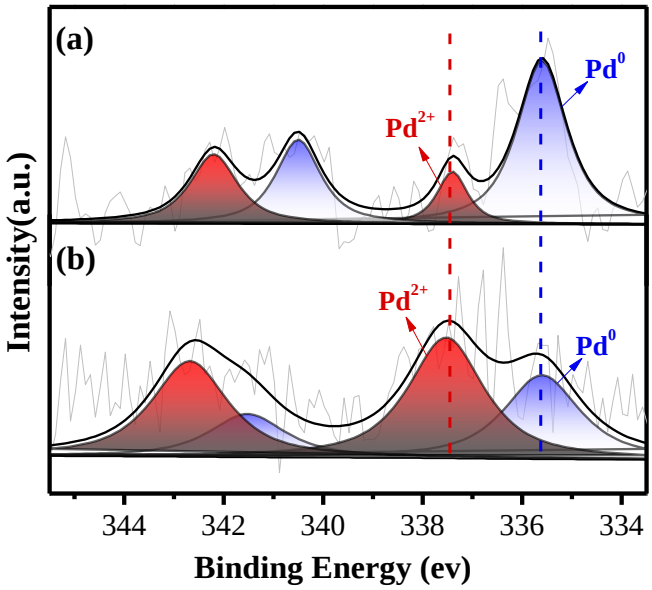

Fig. 8. XPS spectra of Pd 3d of samples (a) $Au_{26}Pd_{74}$/MCF-H_2 (H_2 treatment) and (b) $Au_{26}Pd_{74}$/MCF-O_2 (static air treatment).

Table 2

Binding energies of Au and Pd and atomic ratios of Au/Pd and PdO/Pd.

Samples	Au $4f_{7/2}$(eV)	Pd $3d_{5/2}$ (eV)		Atomic ratio		
		Pd^0 (%)	Pd^{2+} (%)	ICP Au/Pd	XPS Au/Pd	XPS PdO/Pd
Pd_{100}/MCF-H_2	--	-- (0%)	337.2 (100%)	-	-	∞
Au_8Pd_{92}/MCF-H_2	--	336.1 (70%)	337.9 (30%)	0.08	--	0.42
$Au_{18}Pd_{82}$/MCF-H_2	83.7 (84.9)	336.0 (100%)	-- (0%)	0.22	0.22	0
$Au_{26}Pd_{74}$/MCF-H_2	83.7	335.6 (84%)	337.5 (16%)	0.36	0.27	0.19
$Au_{26}Pd_{74}$/MCF-O_2	83.9	335.6 (62%)	337.5 (38%)	0.36	0.14	0.61
$Au_{61}Pd_{39}$/MCF-H_2	83.8	--	--	1.54	--	--

3.7. Catalytic performance

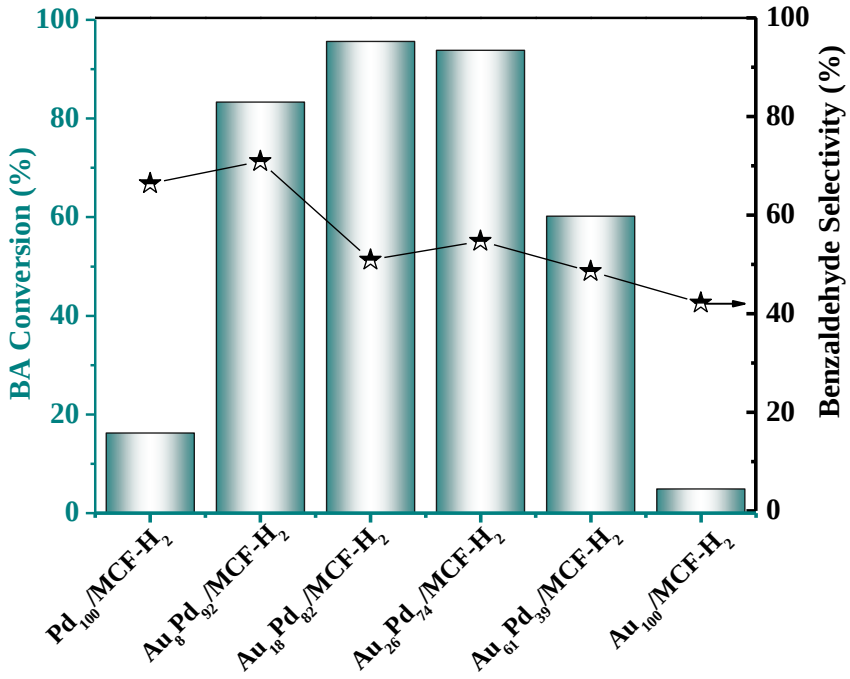

Fig. 9. Selectivity and conversion on catalysts in the benzyl alcohol partial oxidation reaction.

The results for solvent-free oxidation of benzyl alcohol on the Au_xPd_y/MCF-H_2 catalysts are shown in Fig. 9. The comparison of benzyl alcohol oxidation results on the bimetallic Au-Pd catalysts is summarized in Table S1. In this work, the catalytic activity of bimetallic catalysts exhibited a volcano-shape trend across the range of catalysts tested. As shown in Table S1, pure Au and Pd catalysts (samples Au_{100}/MCF-H_2 and Pd_{100}/MCF-H_2) exhibited very low benzyl alcohol conversion studied under the same reaction conditions. Only 4.9 % and 16 % of benzyl alcohol conversion with a TOF of 5000 h^{-1} and 12500h^{-1}on Au_{100}/MCF-H_2 and Pd_{100}/MCF-H_2 catalysts, respectively was obtained. However, a dramatic enhancement of catalytic activity for benzyl alcohol oxidation on bimetallic catalysts was observed, with TOF values of 50000 to 60000 h^{-1}. The benzyl alcohol conversion increased significantly under addition of Au to the Pd catalyst. The highest catalytic activity (TOF = 65700 h^{-1}) was achieved for the $Au_{18}Pd_{82}$/MCF-H_2 catalyst, and it decreased with further increase of the Au/Pd ratio (Table S1). Previously, the highest catalytic activity for benzyl alcohol oxidation (TOF = 63800 h^{-1}) was reported for Au-Pd/C bimetallic catalysts with an Au/Pd molar ratio of nearly 1/2

under similar reaction conditions at 120°C [44], as shown in Table S1. In this work, the highest catalytic activity was achieved for the $Au_{18}Pd_{82}$/MCF-H_2 catalyst with an Au/Pd molar ratio of 1/4.5. The low activity of monometallic Au was due to its inert catalytic activity to alcohol oxidative dehydrogenation and the H-abstraction, which are the rate-determining steps in benzyl alcohol oxidation [12, 45]. And the relative low activity of monometallic Pd catalyst is probably due to the oxidation of surface Pd active sites to PdO. The contiguous Pd islands and Au-Pd interface have been widely accepted as active sites for benzyl alcohol oxidation [46], and Wang et al. revealed that contiguous Pd islands exhibited higher activity for benzyl alcohol activation than separated Pd atoms [16]. Our results confirmed the synergistic effect between Au and Pd for benzyl alcohol oxidation as reported previously [12, 14]. The enhanced catalytic activity of bimetallic Au-Pd catalyst in this work ($Au_{18}Pd_{82}$/MCF-H_2 and $Au_{26}Pd_{74}$/MCF-H_2) is probably due to the formation of a large amount of contiguous Pd islands and a certain amount of Au-Pd interfaces with a low Au/Pd ratio. The catalytic activity decreased dramatically on catalyst $Au_{61}Pd_{39}$/MCF-H_2 with further increasing the Au/Pd ratio. The products distribution on the Au-Pd/MCF catalysts is shown in Table S1. It is clearly seen that different monometallic catalysts lead to completely different products distribution. Catalyst Au_{100}/MCF-H_2 exhibited the lowest benzaldehyde selectivity (42%) among all catalysts with a benzyl alcohol conversion of 4.9%, which is probably due to its inert catalytic activity to benzyl alcohol activation and a free radical reaction may occur. A benzaldehyde selectivity of 66% was obtained on monometallic Pd catalyst with a benzyl alcohol conversion of 16%. The highest benzaldehyde selectivity (>70%) was obtained over the Au_8Pd_{92}/MCF-H_2 with a much higher benzyl alcohol conversion of 83%, indicating that small amount of Au introduced to Pd improved the catalytic activity and benzaldehyde selectivity. However, the benzaldehyde selectivity decreased with further increasing the Au ratio. It was widely accepted that contiguous Pd islands would be active for benzyl alcohol adsorption [16, 46]. Thus, the catalytic activity is proportional to the number of Pd islands. A small amount of Au introduced to Pd created an appropriate amount of Pd islands for benzyl alcohol adsorption,

leading to a high benzyl alcohol conversion and benzaldehyde selectivity over catalyst Au_8Pd_{92}/MCF-H_2. But further increase of the Au ratio leads to higher amount of Pd islands, which promotes benzyl alcohol adsorption, but also impedes the desorption of benzaldehyde [15]. Thus, a balance between benzyl alcohol adsorption and benzaldehyde desorption on Au-Pd core-shell catalyst must be achieved to produce a satisfactory benzaldehyde yield [15]. In this work, the optimum catalyst Au_8Pd_{92}/MCF-H_2 with an Au/Pd ratio of 1/11.5 was obtained.

3.8. Theoretical study: DFT calculations

In order to understand the reactivity of catalysts and surface compositions, DFT calculations were performed. The Pd (111), Pd_3Au (111), and PdO (200) (Fig. S6) surfaces were selected based on the XRD results and studied as model surfaces. The adsorption and desorption properties of reactants (benzyl alcohol and O_2) and products (benzaldehyde and H_2O) were evaluated to explore the essence of synergy effect of Au-Pd alloy NPs. The adsorption configurations are shown in Fig. 10 and Fig. S7-8, the adsorption energies are listed in Table S2.

Top and side views of the adsorption configurations of atomic O(1/2 O_2) on Pd(111), Pd_3Au(111), and PdO(002) are presented in Fig. S7. The obtained adsorption energies of oxygen (adsorption energy of 1/2O_2) on Pd(111), Pd_3Au(111) and PdO(200) surfaces are -0.63 eV, -0.33 eV and -0.75 eV, respectively (see Table S2). Compared with the Pd(111) surface, the oxygen adsorption energy on Pd_3Au(111) is reduced by half, indicating that the formation of gold-palladium alloy can effectively inhibit the adsorption of oxygen on Pd(111) surface to form PdO species, which is consistent with the experimental results. Fig. 10 shows the adsorption/desorption energies and configurations (inset) of benzyl alcohol and H_2O on Pd(111), Pd_3Au(111) and PdO(002) surfaces. The adsorption energies of benzyl alcohol on Pd(111), Pd_3Au(111) and PdO(002) are -1.13 eV, -0.75 eV and -1.06 eV, respectively. The results suggest that Pd_3Au(111) alloy surface has the lowest

adsorption energy to benzyl alcohol. If only the adsorption energy is considered, the activity of the alloy surface should be the lowest. However, it should be noted that the adsorption configurations of benzyl alcohol on different surfaces are different too. Although the benzyl alcohol is adsorbed in parallel on both Pd(111) and $Pd_3Au(111)$ surfaces, it is mainly adsorbed by the benzene ring (π-adsorption) on Pd(111) and primarily by the hydroxyl group on $Pd_3Au(111)$ (Fig. 10). The adsorption via the hydroxyl group on $Pd_3Au(111)$ is beneficial for further activation of O-H bond, which is considered as the first step of benzyl alcohol activation on Pd sites. In addition, the PdO(002) surface presents a strong hydroxyl adsorption, which is probably beneficial for the activation of benzyl alcohol.

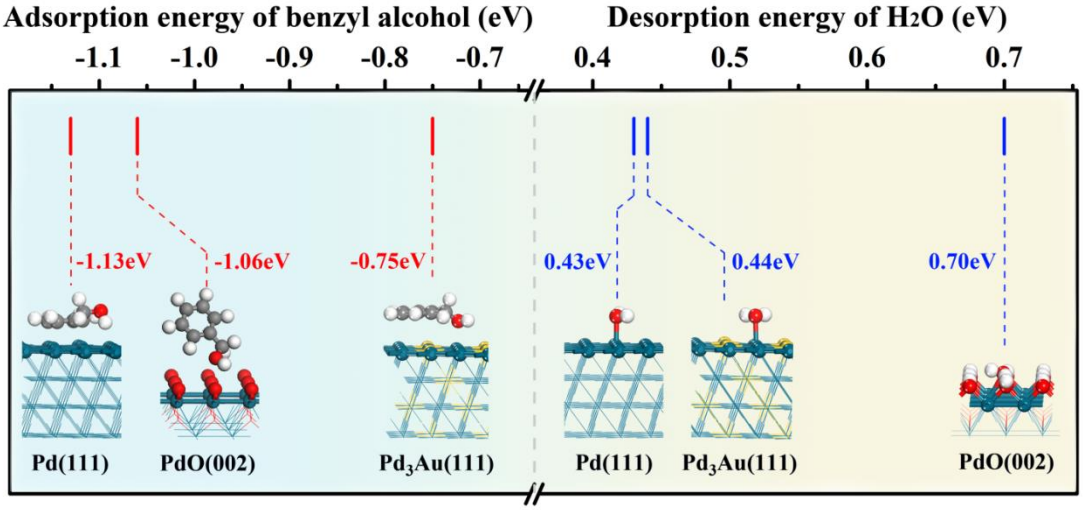

Fig. 10. Adsorption/desorption energies and configurations of benzyl alcohol and H_2O on Pd(111), $Pd_3Au(111)$ and PdO(002) surfaces (blue, yellow, gray, red, and white balls denote Pd Au, C, O, and H atoms, respectively).

The calculated desorption energy of benzaldehyde on Pd(111), $Pd_3Au(111)$ and PdO(002) surfaces are 0.98 eV, 0.46 eV and 0.44 eV, respectively. The benzaldehyde desorption configurations are shown in Fig. S8. The higher desorption energy of benzaldehyde on the Pd(111) surface is unfavorable for the desorption of the reaction product benzaldehyde, which will cause deep oxidation of benzaldehyde and produce a large amount of by-products. Compared with the Pd(111), the desorption energies of benzaldehyde on $Pd_3Au(111)$

and PdO(002) surfaces are reduced significantly, which is beneficial for the desorption of benzaldehyde. As shown in Fig. 10, similar desorption configurations and desorption energies (0.43 eV and 0.44 eV, respectively) of H_2O on Pd(111) and Pd_3Au(111) surfaces were observed. However, DFT calculations suggested that the pure PdO (200) surface easily adsorbs one H atom to form a hydroxyl group but it is difficult to adsorb another H atom and to form a H_2O molecule, because the second hydrogen atom will automatically move to the adjacent oxygen to form another hydroxyl group. It is difficult to form a single water on the PdO(200) surface unless a full surface OH group coverage is obtained. For the hydroxyl groups fully covered the PdO(200) surface, the desorption energy of water molecules is still as high as 0.70 eV (the oxygen atoms of water form a bridge adsorption with Pd, the adsorption distance is 2.518 Å and 2.844 Å). This value is much larger than those on Pd(111) and Pd_3Au(111), indicating the difficulty of H_2O molecule formation and its desorption from the PdO(200). Although the strong hydroxyl adsorption of benzyl alcohol on PdO(002) is beneficial for the activation, the hydrogen produced by hydroxyl cleavage is easy to form a stable -OH on the PdO surface and difficult to form water molecules to desorb, which is detrimental for the following reaction. Therefore, the PdO(002) is an inert surface for catalytic oxidation of benzyl alcohol. This result is consistent with our experimental work demonstrating that the surface enrichment of PdO species leads to a low catalytic activity.

4. Discussion

A volcano-shape activity trend was observed on Au-Pd bimetallic catalysts in the series of samples for benzyl alcohol oxidation tested in this work. Catalyst $Au_{18}Pd_{82}$/MCF-H_2 with the Au/Pd molar ratio of 1/4.5 exhibited much higher benzyl alcohol conversion (96 %) than those of monometallic Au (4.9 %) and Pd (16 %) catalysts. This catalytic activity enhancement was also reported in previous works [14, 43], which was explained as a synergy effect of bimetallic catalyst. Our results confirmed the synergistic effect between Au and Pd for benzyl alcohol oxidation [12, 14], but the reason for this promoting effect is still under debate. No direct evidence for this synergy effect is provided yet.

The focus of this work is to reveal the relationship between the structural properties of bimetallic catalysts and their catalytic performance in benzyl alcohol oxidation reaction. Well dispersed Au-Pd bimetallic NPs with a size in the range of 1-6 nm anchored on the pore wall of foam-like mesoporous silica (> 650 m^2/g) support with addition of MPTMS as a functional ligand were prepared. The Au-Pd alloy NPs were formed under high temperature treatment (500 ^oC) as verified by XRD, UV-Vis and XPS. The surface composition and electronic properties of different catalysts were characterized by XPS and it was found that electron transfer occurred between surface Au and Pd atoms. It is also worth noting that the presence of Au prevents the oxidation of surface Pd atoms, therefore most of the surface Pd species exist as Pd^0 rather than PdO in the Au-Pd alloys. DFT results revealed that the formation of Au-Pd alloy can effectively inhibit the adsorption of oxygen on the Pd(111) surface to form PdO species, consistent with the experimental data. All bimetallic catalysts exhibited much higher catalytic activity for benzyl alcohol oxidation (TOF = 50000 - 60000 h^{-1}) than that of monometallic catalyst Pd_{100}/MCF-H_2 (TOF = 12500 h^{-1}) (Table S1). XPS results also indicated the partial presence and enrichment of PdO species (oxidation of surface Pd atoms) on bimetallic catalysts, leading to a lower Au/Pd ratio at the surface than in the bulk. Correlating the catalytic performance with characterization results, no obvious connection between microstructure of catalysts including specific surface area, pore structure, and NP size with catalytic activity was identified, but a close relationship between surface PdO species and the catalytic activity was observed as shown in Fig. 11. A nearly linear trend indicating that the catalytic activity decreased with the increase of the surface PdO content was observed. The $Au_{18}Pd_{82}$/MCF-H_2 catalyst without any surface PdO species exhibited the highest catalytic activity (TOF = 65700 h^{-1}) among all catalysts, while the Pd_{100}/MCF-H_2 catalyst exhibited much lower catalytic activity (TOF = 12500 h^{-1}) with 100 % surface PdO species. The DFT results confirmed that the $Pd_3Au(111)$ surface of the catalyst favours benzyl alcohol activation and benzaldehyde and H_2O desorption, resulting in a high catalytic activity. However, on the PdO(200) surface, the formation and the desorption of H_2O molecules is very difficult,

leading to a low catalytic activity. These results indicated that the catalytic activity is determined by the state of the surface which is closely related to the Au/Pd ratio. Thus, the relationship between surface PdO content on the Au-Pd bimetallic catalyst and benzyl alcohol oxidation activity is revealed for the first time.

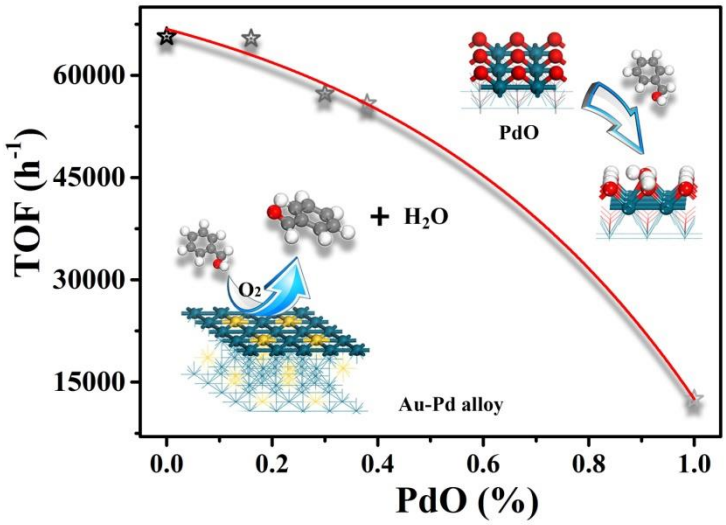

Fig. 11. Relationship between the amount of surface PdO on Au-Pd bimetallic catalysts and their catalytic performance in benzyl alcohol oxidation.

A generally accepted mechanism of benzyl alcohol partial oxidation over Pd-containing catalyst is that the first step is to form the Pd alcoholate intermediate through the O-H bond between the alcohols and Pd sites, followed by the β-hydride elimination [44]. Both the Au-Pd interfaces and low-coordinated Pd^0 islands were considered as active sites for benzyl alcohol oxidation [47]. The surface enrichment of PdO species certainly will decrease or even block the active sites and will affect the catalytic performance. The results of benzyl alcohol oxidation on the $Au_{26}Pd_{74}$/MCF-H_2 and $Au_{26}Pd_{74}$/MCF-O_2 catalysts support this conclusion. After calcination of the catalyst in air ($Au_{26}Pd_{74}$/MCF-O_2), the TOF value decreased dramatically to 55900 h^{-1} in comparison to the TOF of 65700 h^{-1} for the $Au_{26}Pd_{74}$/MCF-H_2 catalyst (Table S1). While similar metal loading, textural structure and Au/Pd bulk ratio were obtained for both catalysts as revealed by STEM-HAADF. The only difference lies in their surface composition as shown in Fig. 8 and Table 2. After oxidation in static air, the surface Pd^{2+} species increased from 16 % on the $Au_{26}Pd_{74}$/MCF-H_2 to 38 % on the $Au_{26}Pd_{74}$/MCF-O_2

catalyst. Meanwhile, the surface Au/Pd atomic ratio decreased from 0.27 to 0.14, and the PdO/Pd ratio increased significantly from 0.19 to 0.61. These results clearly demonstrated that the enrichment of PdO species on catalyst surface decreased the low-coordinated Pd^0 islands and blocked the Au-Pd interface, leading to decreased catalytic activity on the $Au_{26}Pd_{74}$/MCF-O_2 catalyst.

It has been reported that the activity enhancement of Au to Pd atoms is primarily due to the variation of the occupation state of Pd d-orbitals [21]. The occupation state of Pd d-orbitals can be altered by varying the Au/Pd ratio. Different amount of surface PdO species observed on catalysts with different Au/Pd ratios provided the direct evidence in this study. For benzyl alcohol oxidation, the optimal occupation state of Pd d-orbitals was achieved with a Au/Pd ratio of 1/4.5. A significant deviation from this ratio may lead to different occupation states of Pd d-orbitals, resulting in the formation and enrichment of PdO species on the surface with a low catalytic activity.

5. Conclusions

Well dispersed Au-Pd bimetallic (1-6 nm) catalysts supported on foam-like mesoporous silica (specific surface area > 650 m^2/g) were obtained by one-pot synthesis. The formation of Au-Pd alloy NPs and the presence of electron transfer between surface Au and Pd atoms were observed. Both the XPS and DFT results revealed that the addition of Au to Pd prevent the oxidation of surface Pd and formation of PdO species. A volcano-shape activity trend on Au-Pd bimetallic catalyst for benzyl alcohol oxidation was observed. The $Au_{18}Pd_{82}$/MCF-H_2 catalyst with a consistent surface and bulk Au/Pd atomic ratio of 1/4.5 exhibited the highest benzyl alcohol partial oxidation activity. The bimetallic catalysts exhibited greater catalytic activity in benzyl alcohol oxidation (TOF = 50000 - 60000 h^{-1}) compared to the monometallic Pd catalyst (TOF = 12500 h^{-1}). Correlating the catalytic performance with the properties of the catalysts, it was found that high surface PdO content leads to lower catalytic activity. This was further verified by the DFT results revealing that H_2O is difficult to form and desorb from the PdO surface. The overall results provide the direct evidence of synergistic

effect of Au-Pd bimetallic catalyst for benzyl alcohol oxidation. The catalytic activity is determined by surface Au-Pd and low-coordinated Pd atoms. However, the formation and enrichment of inert PdO species on the Au-Pd NPs surfaces result in the decease and blockage of these surface active sites leading to decreased activity. For benzyl alcohol oxidation, an optimal Au/Pd ratio of 1/4.5 was identified and nearly no surface PdO species formation/enrichment was observed, resulting in a high catalytic activity. This study provides new insights on the synergistic effect of Au-Pd bimetallic catalysts and sheds light on the design of bimetallic NPs catalysts for making full use of both Au and Pd atoms.

Acknowledgements

This work was financially supported by the Natural Science Foundation of China (51601223, 21206195), the Fundamental Research Funds for the Central Universities (17CX05018, 17CX02056), Shandong Provincial Natural Science Foundation (ZR201702160196), State Key Laboratory of Heavy Oil Processing （SKLZZ-2017008).

Appendix A. Supplementary data

Supplementary material related to this article can be found, in the online version, at doi:https://doi.org/10.1016/j.apcatb.X.X.X.

References

[1] N. Gogoi, P. Bordoloi, G. Borah, P.K. Gogoi, Synthesis of Palladium Nanoparticle by Bio-reduction Method and Its Effectiveness as Heterogeneous Catalyst Towards Selective Oxidation of Benzyl Alcohols in Aqueous Media, Catal. Lett., 147 (2017) 539-546.

[2] C. Lavenn, A. Demessence, A. Tuel, Au_{25} (SPH-pNH_2)$_{17}$ Nanoclusters Deposited on SBA-15 as Catalysts for Aerobic Benzyl Alcohol Oxidation, J. Catal., 322 (2015) 130-138.

[3] W. Hong, X. Yan, R. Li, J. Fan, Gold Nanoparticle Stabilization Within Tailored Cubic Mesoporous Silica:

Optimizing Alcohol Oxidation Activity, Chin. J. Catal., 38 (2017) 545-553.

[4] A. Lackmann, C. Mahr, M. Schowalter, L. Fitzek, J. Weissmueller, A. Rosenauer, A. Wittstock, A Comparative Study of Alcohol Oxidation over Nanoporous Gold in Gas and Liquid Phase, J. Catal., 353 (2017) 99-106.

[5] N. Liu, G. Chen, W. Dong, C. Liu, C. Xu, Preparation of Au Nanoparticles with High Dispersion and Thermal Stability by A Controlled Impregnation Method for Alcohol Oxidation, Gold Bulletin, 50 (2017) 163-175.

[6] S. Campisi, D. Ferri, A. Villa, W. Wang, D. Wang, O. Krocher, L. Prati, Selectivity Control in Palladium-Catalyzed Alcohol Oxidation through Selective Blocking of Active Sites, J. Phys. Chem. C, 120 (2016) 14027-14033.

[7] A. Savara, C.E. Chan-Thaw, I. Rossetti, A. Villa, L. Prati, Benzyl Alcohol Oxidation on Carbon-Supported Pd Nanoparticles: Elucidating the Reaction Mechanism, Chemcatchem, 6 (2014) 3464-3473.

[8] F. Gomez-Villarraga, J. Radnik, A. Martin, A. Koeckritz, Synergistic Effect in the Oxidation of Benzyl Alcohol Using Citrate-Stabilized Gold Bimetallic Nanoparticles Supported on Alumina, J. Nanopart. Res., 18 (2016) 31-38.

[9] C.M. Olmos, L.E. Chinchilla, E.G. Rodrigues, J.J. Delgado, A.B. Hungría, G. Blanco, M.F. Pereira, J.J. Órfão, J.J. Calvino, X. Chen, Synergistic Effect of Bimetallic Au-Pd Supported on Ceria-zirconia Mixed Oxide Catalysts for Selective Oxidation of Glycerol, Appl. Catal. B: Environ., 197 (2016) 222-235.

[10] N. Al-Rifai, F. Galvanin, M. Morad, E. Cao, S. Cattaneo, M. Sankar, V. Dua, G. Hutchings, A. Gavriilidis, Hydrodynamic Effects on Three Phase Micro-packed Bed Reactor Performance - Gold-Palladium Catalysed Benzyl Alcohol Oxidation, Chem. Eng. Sci., 149 (2016) 129-142.

[11] S. Cheong, L. Graham, G.L. Brett, A.M. Henning, J. Watt, P.J. Miedziak, M. Song, Y. Takeda, S.H. Taylor, R.D. Tilley, Au-Pd Core-Shell Nanoparticles as Alcohol Oxidation Catalysts: Effect of Shape and

Composition, ChemSusChem, 6 (2013) 1858-1862.

[12] C.M. Olmos, L.E. Chinchilla, A. Villa, J.J. Delgado, H. Pan, A.B. Hungria, G. Blanco, J.J. Calvino, L. Prati, X. Chen, Influence of Pretreatment Atmospheres on the Performance of Bimetallic Au-Pd Supported on Ceria-zirconia Mixed Oxide Catalysts for Benzyl Alcohol Oxidation, Appl. Catal. A-Gen., 525 (2016) 145-157.

[13] T. Jiang, C. Jia, L. Zhang, S. He, Y. Sang, H. Li, Y. Li, X. Xu, H. Liu, Gold and Gold-palladium Alloy Nanoparticles on Heterostructured TiO_2 Nanobelts as Plasmonic Photocatalysts for Benzyl Alcohol Oxidation, Nanoscale, 7 (2015) 209-217.

[14] J.H. Carter, S. Althahban, E. Nowicka, S.J. Freakley, D.J. Morgan, P.M. Shah, S. Golunski, C.J. Kiely, G.J. Hutchings, Synergy and Anti-Synergy between Palladium and Gold in Nanoparticles Dispersed on a Reducible Support, ACS Catal., 6 (2016) 6623-6633.

[15] T.A.G. Silva, E. Teixeira-Neto, N. Lopez, L.M. Rossi, Volcano-like Behavior of Au-Pd Core-shell Nanoparticles in the Selective Oxidation of Alcohols, Sci. Rep., 4 (2014) 1-5.

[16] H. Wang, C. Wang, H. Yan, H. Yi, J. Lu, Precisely-controlled Synthesis of Au@Pd Core-shell Bimetallic Catalyst via Atomic Layer Deposition for Selective Oxidation of Benzyl Alcohol, J. Catal., 324 (2015) 59-68.

[17] H. Zhang, T. Watanabe, M. Okumura, M. Haruta, N. Toshima, Catalytically Highly Active Top Gold Atom on Palladium Nanocluster, Nat. Mater., 11 (2012) 49-52.

[18] J. Long, H. Liu, S. Wu, S. Liao, Y. Li, Selective Oxidation of Saturated Hydrocarbons Using Au-Pd Alloy Nanoparticles Supported on Metal-Organic Frameworks, ACS Catal., 3 (2013) 647-654.

[19] X. Wei, X.-F. Yang, A.-Q. Wang, L. Li, X.-Y. Liu, T. Zhang, C.-Y. Mou, J. Li, Bimetallic Au-Pd Alloy Catalysts for N_2O Decomposition: Effects of Surface Structures on Catalytic Activity, J. Phys. Chem. C, 116 (2012) 6222-6232.

[20] F. Gao, D.W. Goodman, Pd–Au Bimetallic Catalysts: Understanding Alloy Effects from Planar Models

and (supported) Nanoparticles, Chem. Soc. Rev., 41 (2012) 8009-8020.

[21] R. Liu, H.-m. Chen, L.-p. Fang, C. Xu, Z. He, Y. Lai, H. Zhao, D. Bekana, J.-f. Liu, Au@ Pd Bimetallic Nanocatalyst for Carbon–Halogen Bond Cleavage: An Old Story with New Insight into How the Activity of Pd is Influenced by Au, Environ. Sci. Technol., 52 (2018) 4244-4255.

[22] Y. Han, S.S. Lee, J.Y. Ying, Spherical Siliceous Mesocellular Foam Particles for High-speed Size Exclusion Chromatography, Chem. Mater., 19 (2007) 2292-2298.

[23] K. An, N. Musselwhite, G. Kennedy, V.V. Pushkarev, L.R. Baker, G.A. Somorjai, Preparation of Mesoporous Oxides and Their Support Effects on Pt Nanoparticle Catalysts in Catalytic Hydrogenation of Furfural, J.Colloid Interf. Sci., 392 (2013) 122-128.

[24] P. Wu, P. Bai, K.P. Loh, X. Zhao, Au Nanoparticles Dispersed on Functionalized Mesoporous Silica for Selective Oxidation of Cyclohexane, Catal. Today, 158 (2010) 220-227.

[25] P. Wu, P. Bai, Z. Yan, G.X. Zhao, Gold Nanoparticles Supported on Mesoporous Silica: Origin of High Activity and Role of Au NPs in Selective Oxidation of Cyclohexane, Sci. Rep., 6 (2016) 18817-18828.

[26] M. López‐Haro, J.J. Delgado, J.M. Cies, E. del Rio, S. Bernal, R. Burch, M.A. Cauqui, S. Trasobares, J.A. Pérez‐Omil, P. Bayle‐Guillemaud, Bridging the Gap Between CO Adsorption Studies on Gold Model Surfaces and Supported Nanoparticles, Angew. Chem. Int. Ed., 49 (2010) 1981-1985.

[27] M. Thommes, K. Kaneko, A.V. Neimark, J.P. Olivier, F. Rodriguez-Reinoso, J. Rouquerol, K.S. Sing, Physisorption of Gases, with Special Reference to the Evaluation of Surface Area and Pore Size Distribution (IUPAC Technical Report), Pure Appl. Chem., 87 (2015) 1051-1069.

[28] H. Yang, J. Deng, Y. Liu, S. Xie, Z. Wu, H. Dai, Preparation and Catalytic Performance of Ag, Au, Pd or Pt Nanoparticles Supported on 3DOM CeO_2-Al_2O_3 for Toluene Oxidation, J. Mol. Catal. A-Chem., 414 (2016) 9-18.

[29] S. Xie, J. Deng, S. Zang, H. Yang, G. Guo, H. Arandiyan, H. Dai, Au-Pd/3DOM Co_3O_4: Highly Active

and Stable Nanocatalysts for Toluene Oxidation, J. Catal., 322 (2015) 38-48.

[30] J. Luo, M.M. Maye, V. Petkov, N.N. Kariuki, L.Y. Wang, P. Njoki, D. Mott, Y. Lln, C.J. Zhong, Phase Properties of Carbon-supported Gold-platinum Nanoparticles with Different Bimetallic Compositions, Chem. Mater., 17 (2005) 3086-3091.

[31] R. Tiruvalam, J. Pritchard, N. Dimitratos, J. Lopez-Sanchez, J. Edwards, A. Carley, G. Hutchings, C. Kiely, Aberration Corrected Analytical Electron Microscopy Studies of Sol-immobilized Au^{+} Pd, Au {Pd} and Pd {Au} Catalysts Used for Benzyl Alcohol Oxidation and Hydrogen Peroxide Production, Faraday Discuss., 152 (2011) 63-86.

[32] J. Sa, S.F.R. Taylor, H. Daly, A. Goguet, R. Tiruvalam, Q. He, C.J. Kiely, G.J. Hutchings, C. Hardacre, Redispersion of Gold Supported on Oxides, ACS Catal., 2 (2012) 552-560.

[33] P. Wu, Z. Xiong, K.P. Loh, X. Zhao, Selective Oxidation of Cyclohexane over Gold Nanoparticles Supported on Mesoporous Silica Prepared in the Presence of Thioether Functionality, Catal. Sci. Technol., 1 (2011) 285-294.

[34] A. Venezia, V. La Parola, V. Nicolı, G. Deganello, Effect of Gold on the HDS Activity of Supported Palladium Catalysts, J. Catal., 212 (2002) 56-62.

[35] S. Deki, K. Akamatsu, Y. Hatakenaka, M. Mizuhata, A. Kajinami, Synthesis and Characterization of Nano-sized Gold-palladium Bimetallic Particles Dispersed in Polymer Thin Film Matrix, Nanostruct. Mater., 11 (1999) 59-65.

[36] A. Venezia, L. Liotta, G. Pantaleo, V. La Parola, G. Deganello, A. Beck, Z. Koppány, K. Frey, D. Horvath, L. Guczi, Activity of SiO_2 Supported Gold-palladium Catalysts in CO Oxidation, Appl. Catal. A: Gen., 251 (2003) 359-368.

[37] A.A. Herzing, C.J. Kiely, A.F. Carley, P. Landon, G.J. Hutchings, Identification of Active Gold Nanoclusters on Iron Oxide Supports for CO Oxidation, Science, 321 (2008) 1331-1335.

[38] X. Li, S.S.S. Fang, J. Teo, Y.L. Foo, A. Borgna, M. Lin, Z. Zhong, Activation and Deactivation of Au-Cu/SBA-15 Catalyst for Preferential Oxidation of CO in H_2-Rich Gas, ACS Catal., 2 (2012) 360-369.

[39] P. Wu, P. Bai, W. Xia, X. Yang, J. Li, Z. Yan, One-Pot Synthesis of Silica Supported Au–Ag Alloy Nanoparticles for Cyclohexane Oxidation, Nanosci. Nanotech. Lett., 8 (2016) 972-977.

[40] S. Sarina, S. Bai, Y. Huang, C. Chen, J. Jia, E. Jaatinen, G.A. Ayoko, Z. Bao, H. Zhu, Visible Light Enhanced Oxidant Free Dehydrogenation of Aromatic Alcohols Using Au-Pd Alloy Nanoparticle Catalysts, Green Chem., 16 (2014) 331-341.

[41] T. Teranishi, M. Miyake, Size Control of Palladium Nanoparticles and Their Crystal Structures, Chem. Mater., 10 (1998) 594-600.

[42] R.J. Farrauto, J.K. Lampert, M.C. Hobson, E.M. Waterman, Thermal Decomposition and Reformation of PdO Catalysts: Support Effects, Appl.Catal. B: Environ., 6 (1995) 263-270.

[43] X. Yang, D. Chen, S. Liao, H. Song, Y. Li, Z. Fu, Y. Su, High-performance Pd-Au Bimetallic Catalyst with Mesoporous Silica Nanoparticles as Support and its Catalysis of Cinnamaldehyde Hydrogenation, J. Catal., 291 (2012) 36-43.

[44] Q. He, P.J. Miedziak, L. Kesavan, N. Dimitratos, M. Sankar, J.A. Lopez-Sanchez, M.M. Forde, J.K. Edwards, D.W. Knight, S.H. Taylor, C.J. Kiely, G.J. Hutchings, Switching-off Toluene Formation in the Solvent-free Oxidation of Benzyl Alcohol Using Supported Trimetallic Au-Pd-Pt Nanoparticles, Faraday Discuss., 162 (2013) 365-378.

[45] T. Mallat, A. Baiker, Oxidation of Alcohols with Molecular Oxygen on Solid Catalysts, Chem. Rev., 104 (2004) 3037-3058.

[46] S. Han, C.B. Mullins, Surface Alloy Composition Controlled O_2 Activation on Pd–Au Bimetallic Model Catalysts, ACS Catal., 8 (2018) 3641-3649.

[47] Y. Chen, H. Wang, C.-J. Liu, Z. Zeng, H. Zhang, C. Zhou, X. Jia, Y. Yang, Formation of Monometallic

Au and Pd and Bimetallic Au–Pd Nanoparticles Confined in Mesopores via Ar Glow-discharge Plasma Reduction and their Catalytic Applications in Aerobic Oxidation of Benzyl Alcohol, J. Catal., 289 (2012) 105-117.